

MultiXNet: Multiclass Multistage Multimodal Motion Prediction

Nemanja Djuric, Henggang Cui, Zhaoen Su, Shangxuan Wu, Huahua Wang,
Fang-Chieh Chou, Luisa San Martin, Song Feng, Rui Hu, Yang Xu, Alyssa Dayan,
Sidney Zhang, Brian C. Becker, Gregory P. Meyer, Carlos Vallespi-Gonzalez, Carl K. Wellington
Uber Advanced Technologies Group

{ndjuric, hcui2, suzhaoen, shangxuan.wu, anteaglewang, fchou, luisasm}@uber.com
{songf, rui.hu, yang.xu, ada, sidney, bbecker, gmeyer, cvallespi, cwellington}@uber.com

Abstract—One of the critical pieces of the self-driving puzzle is understanding the surroundings of the self-driving vehicle (SDV) and predicting how these surroundings will change in the near future. To address this task we propose MultiXNet, an end-to-end approach for detection and motion prediction based directly on lidar sensor data. This approach builds on prior work by handling multiple classes of traffic actors, adding a jointly trained second-stage trajectory refinement step, and producing a multimodal probability distribution over future actor motion that includes both multiple discrete traffic behaviors and calibrated continuous uncertainties. The method was evaluated on a large-scale, real-world data set collected by a fleet of SDVs in several cities, with the results indicating that it outperforms existing state-of-the-art approaches.

I. INTRODUCTION

Predicting the future states of other actors such as vehicles, pedestrians, and bicyclists represents a key capability for self-driving technology. This is a challenging task, and has been found to play an important role in accident avoidance for human drivers [1], [2], as well as for their autonomous counterparts [3]. Within the context of a Self-Driving Vehicle (SDV) it is important to capture the range of possibilities for other actors, and not just a single most likely trajectory. Consider an opposing vehicle approaching an intersection, which may continue driving straight or turn in front of the SDV. In order to ensure safety the SDV needs to accurately reason about both of these possible modes and modulate its behavior accordingly. In addition to the discrete modes, a downstream motion planner may react differently to a prediction depending on the continuous uncertainty within a predicted trajectory. As an example, if an opposing vehicle looks like it might take a wide turn and come into the SDV's lane, the SDV can preemptively slow down to reduce the risk. On the other hand, if the prediction shows confidence that the opposing vehicle will stay in its lane the SDV could choose to maintain its current speed.

Bringing the above requirements together, Fig. 1 shows an example of the task addressed by this work. The input is a map and a sequence of lidar data which is projected into a common global coordinate frame using the SDV pose. The output is a multimodal distribution over potential future states for the other actors in the scene. An important challenge is that various actor types such as pedestrians and vehicles exhibit significantly different behavior, while a deployed approach needs to handle all actors present in a scene.

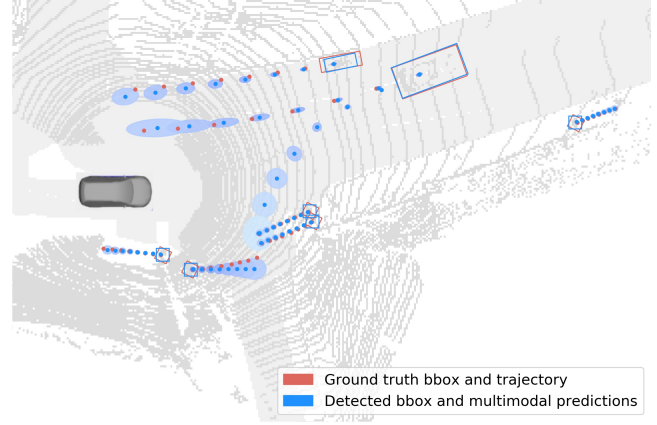


Fig. 1: Example output of the proposed MultiXNet model, showing detections and multimodal, uncertainty-aware motion predictions for multiple actor types overlaid on top of lidar and map data (including pedestrians on the sidewalks and a vehicle and a bicyclist approaching the SDV)

Prior work in this area has demonstrated strong performance by using end-to-end methods that jointly learn detection and motion prediction directly from sensor data [4], [5], including the addition of a jointly learned refinement stage of the network that leads to improved trajectory prediction [6]. However, these approaches have generally focused only on vehicles and produce a single trajectory rather than full motion distributions. More recent work has shown the ability to learn a continuous distribution directly from sensor data for multiple classes [7], but the distributions are not multimodal. Prediction methods that operate on detections rather than the raw sensor data have shown improved performance by introducing multiclass predictions [8], estimates of uncertainty [9], [10], or incorporating multiple modes [11]. While each of these concepts has been considered individually, this work looks to unify them into a single approach which we empirically show to outperform the competing baselines.

Our work builds on IntentNet [5] to produce an end-to-end approach for motion prediction from lidar data with the following contributions:

- joint detection and motion prediction of multiple actor classes: vehicles, pedestrians, and bicyclists;
- modeling both cross-track and along-track uncertainty of actor movement;

- a jointly trained second-stage trajectory refinement step that improves prediction accuracy;
- multimodal trajectory prediction to capture distinct future trajectories of traffic actors.

Using a large-scale, real-world data set, the proposed approach was shown to outperform the current state-of-the-art, and we experimentally demonstrate the contribution of each of the above improvements.

II. RELATED WORK

Object detection is a critical task for a SDV system, with a number of papers proposed recently in the literature. A popular approach is using a bird’s-eye view (BEV) representation, where lidar points are encoded in 3D voxels [5], which has a strong benefit of being a range-invariant representation of objects. PointPillars [12] proposed to learn the BEV encoding through a computation scheme that provides better speed while keeping accuracy high. Range view (RV) is another popular lidar point representation which provides a compact input while preserving all sensor information. The authors of [13] showed that RV is good at detection of both near and long-range objects, which can further be improved by combining a camera image with RV lidar [14]. Recent work applies both BEV and RV representations [15], [16], extracting features using separate branches of the network that are fused at a later stage. This fusion method preserves information for both near- and long-range objects, at the cost of a more complex and heavy network structure. In this work we focus on a BEV approach, and discuss several ideas for how to improve on the current state-of-the-art.

Movement prediction is another major topic in the SDV community. Typically, the prediction models take current and past detections as inputs, and then output trajectories for the next several seconds. A common approach is to train recurrent models to process the inputs and extract learned features [17], [18], [19], [20], [21], [22], [23]. A number of methods have been proposed that take actor surroundings and other contextual information through BEV images as input, and extract useful scene features using convolutional neural networks (CNNs) [4], [8], [9], [10], [11], [19]. These models can then predict actor trajectories using a decoder architecture based on the extracted features. Interestingly, the majority of former research on trajectory prediction has focused on predicting the motion of a particular type of road actor (e.g., vehicle or pedestrian). However, multiple types of traffic actors exist together on public roads, and SDVs need to accurately predict all relevant actors’ motions in order to drive safely. Moreover, different actor types have distinct motion patterns (e.g., bicyclists and pedestrians behave quite differently [8]), and it is important to model them separately. A few recent papers tackled this challenge using recurrent methods [19], [24], [25], however unlike our work an existence of a detection system was assumed and they were not trained end-to-end using raw sensor data.

Another aspect of the prediction task that is important for ensuring safe SDV operations is modeling the stochasticity of traffic behavior, either by considering multimodality of

actor movement (e.g., whether they are going to turn left or right at an intersection) or position uncertainty within a single mode. When it comes to multimodality of future trajectories there are two common classes of approaches. The first is the use of generative models, either explicitly with conditional variational autoencoders [17], [18], [19], [26] or implicitly with generative adversarial networks [20], [21], [22], [23]. Once trained, trajectories are predicted by sampling from the learned distribution at inference time. The generative models often require the system to draw many samples to ensure good coverage in the trajectory space (e.g., as many as 20 for [20], [22]), which may be impractical for time-critical applications. The second category of approaches directly predicts a fixed number of trajectories along with their probabilities in a single-shot manner [9], [11], [27], [28]. The trajectories and probabilities are jointly trained with a combination of regression and classification losses, and are much more efficient than the alternatives. As a result, most applied work follows the one-shot approach [9], [27].

In addition to multimodality, it is important to capture uncertainty of actor motion within a trajectory mode. This can be achieved by explicitly modeling each trajectory as a probability distribution, for example by modelling trajectory waypoints using Gaussians [9], [10], [18], [19], [29]. Following a different paradigm, some researchers have proposed non-parametric approaches [30] to directly predict an occupancy map. While parametric approaches can easily be cast into cell occupancy space the reverse is not necessarily true, limiting the applicability of such output representations in downstream modules of the SDV system.

Instead of using independent detection and motion forecasting models, some recent work has proposed to train them jointly in an end-to-end fashion, taking raw sensor data as inputs. This approach was pioneered in the FaF model [4], while IntentNet [5] further included map data as an input and proposed to predict both actor trajectories and their high-level intents. The authors of [31] further extended this idea to an end-to-end model that also includes motion planning. SpAGNN [6] introduced a two-stage model with Rotated Region of Interest (RROI) cropping, a graph neural network module to encode actor relations, as well as modeling the uncertainty of future trajectories. MotionNet [32] used a spatial-temporal pyramid network to jointly perform detection and motion prediction for each BEV grid cell. LaserFlow [7] proposed an end-to-end model using multi-frame RV lidar inputs, unlike the other methods which use BEV representations, which can also perform prediction on multiple actor types. Compared to our method, most of the above end-to-end methods do not consider motion prediction on diverse road actor types, and none of them addresses the multimodal nature of possible future trajectories. The earlier work has clearly shown the promise of end-to-end approaches, with researchers looking at various aspects to improve the prediction performance. In this paper we propose the first model to bring these key ideas together, and show in the experimental section the benefits over the baselines.

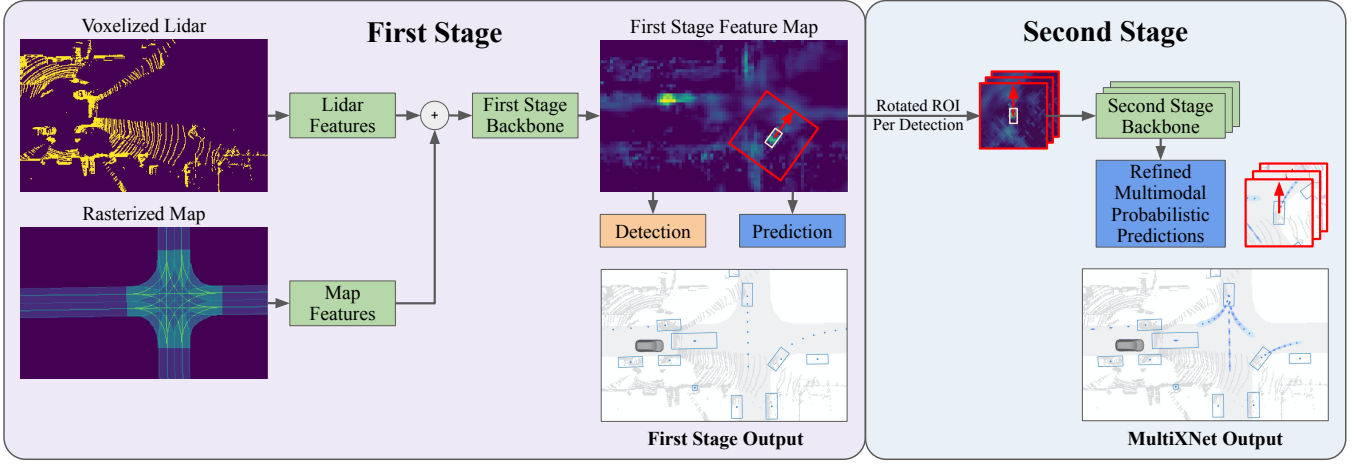


Fig. 2: Overview of the MultiXNet architecture, where the first-stage network corresponding to IntentNet [5] outputs actor detections and their unimodal motion prediction, while the second stage refines predictions to be multimodal and uncertainty-aware; note that the first-stage prediction of the right-turning vehicle is incorrect, and the second stage improves its prediction

III. PROPOSED APPROACH

In this section we describe our end-to-end method for joint detection and prediction, called MultiXNet. We first describe the existing state-of-the-art IntentNet architecture [5], followed by a discussion of our proposed improvements.

A. Baseline end-to-end detection and prediction

1) *Input representation*: In Fig. 2 we show the lidar and map inputs to the network. We assume a lidar sensor installed on the SDV that provides measurements at regular time intervals. At time t a lidar sweep \mathcal{S}_t comprises a set of 3D lidar returns represented by their (x, y, z) locations. Following [5], we encode the lidar data \mathcal{S}_t in a BEV image centered on the SDV, with voxel sizes of Δ_L and Δ_W along the forward x - and left y -axes, respectively, and Δ_V along the vertical axis (representing the image channels). Each voxel encodes binary information about whether or not there exists at least one lidar return inside that voxel. In addition, to capture temporal information we encode the $T - 1$ past lidar sweeps $\{\mathcal{S}_{t-T+1}, \dots, \mathcal{S}_{t-1}\}$ into the same BEV frame using their known SDV poses, and stack them together along the channel (or vertical) dimension. Assuming we consider an area of length L , width W , and height V , this yields an image of size $\left\lceil \frac{L}{\Delta_L} \right\rceil \times \left\lceil \frac{W}{\Delta_W} \right\rceil \times T \left\lceil \frac{V}{\Delta_V} \right\rceil$.

Moreover, let us assume we have access to a high-definition map of the operating area around the SDV denoted by \mathcal{M} . As shown in Fig. 2, we encode static map elements from \mathcal{M} in the same BEV frame as introduced above. These include driving paths, crosswalks, lane and road boundaries, intersections, driveways, and parking lots, where each element is encoded as a binary mask in its own separate channel. This results in a total of seven map additional channels, which are processed by a few convolutional layers before being stacked with the processed lidar channels, to be used as a BEV input to the rest of the network, as described in [5].

2) *Network architecture and output*: The input BEV image can be viewed as a top-down grid representation of the SDV's surroundings, with each grid cell comprising input features encoded along the channel dimensions. As in [5], this image is then processed by a sequence of 2-D convolutional layers to produce a final layer that contains learned features for each cell location. Following an additional 1×1 convolutional layer, for each cell we predict two sets of outputs, representing object detection and its movement prediction (in the following text we denote a predicted value by the hat-notation $\hat{\cdot}$). In particular, the detection output for a cell centered at (x, y) comprises an existence probability \hat{p} , oriented bounding box represented by its center $\hat{\mathbf{c}}_0 = (\hat{c}_{x0}, \hat{c}_{y0})$ relative to the center of the grid cell, size represented by length \hat{l} and width \hat{w} , and heading $\hat{\theta}_0$ relative to the x -axis, parameterized as a tuple $(\sin \hat{\theta}_0, \cos \hat{\theta}_0)$. In addition, the prediction output is composed of bounding box centers (or waypoints) $\hat{\mathbf{c}}_h = (\hat{c}_{xh}, \hat{c}_{yh})$ and headings $\hat{\theta}_h$ at H future time horizons, with $h \in \{1, \dots, H\}$. A full set of H waypoints is denoted as a trajectory $\hat{\tau} = \{\hat{\mathbf{c}}_h, \hat{\theta}_h\}_{h=1}^H$, where the bounding box size is considered constant across the entire prediction horizon.

3) *Loss*: As discussed in [5], the loss at a certain time step consists of detection and prediction losses computed over all BEV cells. When it comes to the per-pixel detection loss, a binary focal loss $\ell_{focal}(\hat{p}) = (1 - \hat{p})^\gamma \log \hat{p}$ is used for the probability of a ground-truth object [33], where we empirically found good performance with hyper-parameter γ set to 2. Moreover, when there exists a ground-truth object in a particular cell a smooth- ℓ_1 regression loss $\ell_1(\hat{v} - v)$ is used for all bounding box parameters (i.e., center, size, and heading), where the loss is computed between the predicted value \hat{v} and the corresponding ground truth v . The smooth- ℓ_1 regression loss is used to capture prediction errors of future bounding box centers and headings. We refer to a cell containing an object as a *foreground* (fg) cell, and a *background* (bg) cell otherwise. Then, the overall loss at

horizon h for a foreground cell $\mathcal{L}_{fg(h)}$ is computed as

$$\begin{aligned} \mathcal{L}_{fg(h)} = & 1_{h=0} \left(\ell_{focal}(\hat{p}) + \ell_1(\hat{l} - l) + \ell_1(\hat{w} - w) \right) + \\ & \ell_1(\hat{c}_{xh} - c_{xh}) + \ell_1(\hat{c}_{yh} - c_{yh}) + \\ & \ell_1(\sin\hat{\theta}_h - \sin\theta_h) + \ell_1(\cos\hat{\theta}_h - \cos\theta_h), \end{aligned} \quad (1)$$

where 1_c equals 1 if the condition c holds and 0 otherwise. Loss for a background cell equals $\mathcal{L}_{bg} = \ell_{focal}(1 - \hat{p})$.

Lastly, to enforce a lower error tolerance for earlier horizons we multiply the per-horizon losses by fixed weights that are gradually decreasing for future timesteps, and the per-horizon losses are aggregated to obtain the final loss,

$$\mathcal{L} = 1_{bg \text{ cell}} \mathcal{L}_{bg} + 1_{fg \text{ cell}} \sum_{h=0}^H \lambda^h \mathcal{L}_{fg(h)}, \quad (2)$$

where $\lambda \in (0, 1)$ is a constant decay factor (set to 0.97 in our experiments). The loss contains both detection and prediction components, and all model parameters are learned jointly in an end-to-end manner.

B. Improving end-to-end motion prediction

In this section we present an end-to-end method that improves over the current state-of-the-art. We build on the approach presented in the previous section, extending it to significantly improve its motion prediction performance.

1) *Uncertainty-aware loss*: In addition to predicting trajectories, an important task in autonomous driving is the estimation of their spatial uncertainty. This is useful for fusion of results from multiple predictors, and is also consumed by a motion planner to improve SDV safety. In earlier work [10] it was proposed as a fine-tuning step following training of a model that only considered trajectory waypoints without uncertainties. Then, by freezing the main prediction weights or setting a low learning rate, the uncertainty module was trained without hurting the overall prediction performance.

In this paper we describe a method that learns trajectories and uncertainties jointly, where we decompose the position uncertainty in the along-track (AT) and cross-track (CT) directions [34]. In particular, a predicted waypoint \hat{c}_h is projected along AT and CT directions by considering the ground-truth heading θ_h , and the errors along these directions are assumed to follow a Laplace distribution $Laplace(\mu, b)$, with a PDF of a random Laplacian variable v computed as

$$\frac{1}{2b} \exp\left(-\frac{|v - \mu|}{b}\right), \quad (3)$$

where mean μ and diversity b are the Laplace parameters. We assume that AT and CT errors are independent, with each having a separate set of Laplace parameters. Taking AT as an example and assuming an error value \hat{e}_{AT} , this defines a Laplace distribution $Laplace(\hat{e}_{AT}, \hat{b}_{AT})$. Then, we minimize the loss by minimizing the Kullback–Leibler (KL) divergence between the ground-truth $Laplace(0, b_{AT})$ and the predicted $Laplace(\hat{e}_{AT}, \hat{b}_{AT})$, computed as follows [35],

$$KL_{AT} = \log \frac{\hat{b}_{AT}}{b_{AT}} + \frac{b_{AT} \exp\left(-\frac{|\hat{e}_{AT}|}{b_{AT}}\right) + |\hat{e}_{AT}|}{\hat{b}_{AT}} - 1. \quad (4)$$

Similarly, KL_{CT} can be computed for the CT errors, and we then use KL_{AT} and KL_{CT} instead of the smooth- ℓ_1 loss for bounding box centers introduced in the previous section.

An important question is the choice of ground-truth diversities b_{AT} and b_{CT} . In earlier detection work [36] a percentage of label area covered by lidar points was used, however this may not be the best choice for the prediction task as the prediction difficulty and uncertainty is expected to grow with longer horizons. To account for this, we linearly increase the ground-truth diversity with time,

$$b_*(t) = \alpha_* + \beta_* t, \quad (5)$$

where parameters α_* and β_* are empirically determined, with separate parameters for AT and for CT components. This is achieved by training models with varying α_* and β_* parameters and choosing the parameter set for which the reliability diagrams [10] indicate that the model outputs are the most calibrated, discussed in Sec. IV-B.

2) *Second-stage trajectory refinement*: As shown in Fig. 2, following the detection and prediction inference described in Sec. III-A we perform further refinement of the motion predictions for the detected objects. The refinement network, which we refer to as the *second stage* of the model, discards the first-stage trajectory predictions and takes the inferred object center \hat{c}_0 and heading $\hat{\theta}_0$, as well as the final feature layer from the main network. Then, it crops and rotates learned features for each actor, such that the actor is oriented pointing up in the rotated image [8], [10], [37] as illustrated in Fig. 2. The RROI feature map is then fed through a lightweight CNN network before the final prediction of future trajectory and uncertainty is performed. Both first- and second-stage networks are trained jointly, using the full loss \mathcal{L} in the first stage and only the future prediction loss in the second stage, where the second-stage predictions are used as the final output trajectories.

The proposed method has several advantages. First, the output representation can be standardized in the actor frame. In the first-stage model the output trajectories can radiate in any direction from the actor position, while in the actor frame the majority of the future trajectories grow from the origin forward. In addition, the second stage network can concentrate on extracting features for a single actor of interest and discard irrelevant information. It is important to clarify that the purpose of a two-stage approach is different from that in Faster R-CNN [38], where it was used to refine and classify region proposals. Instead, in our work the second stage is used to refine the trajectories and not the detections.

3) *Multimodal trajectory prediction*: Traffic behavior is inherently multimodal, as traffic actors at any point may make one of several movement decisions. Modeling such behavior is an important task in the self-driving field, with several interesting ideas being proposed in the literature [9], [11], [27], [28]. In this paper we address this problem, and describe an approach to output a fixed number of trajectories for each detected actor along with their probabilities. In particular, instead of outputting a single predicted trajectory in the second stage for each detected actor, the model

outputs a fixed number of M trajectories. Let us denote trajectory modes output by the model as $\{\hat{\tau}_m\}_{m=1}^M$, and their probabilities $\{\hat{p}_m\}_{m=1}^M$. First, we identify one of the M modes as the *ground-truth mode* m_{gt} , for which purpose we designed a novel direction-based policy to decide the ground-truth mode. More specifically, we compute an angle $\Delta_\theta = \theta_H - \theta_0$ between the last and the current ground-truth heading, where $\Delta_\theta \in (-\pi, \pi]$. Then, we divide the range $(-\pi, \pi]$ into M bins and decide m_{gt} based on where Δ_θ falls. In this way, during training each mode is specialized to be responsible for a distinct behavior (e.g., for $M = 3$ we have left-turning, right-turning, and going-straight modes).

Given the predictions and the ground-truth trajectory, and using a similar approach as discussed in [11], the multimodal trajectory loss consists of a trajectory loss of the m_{gt} -th trajectory mode as described in Sec. III-B.1 and a cross-entropy loss for the trajectory probabilities. Lastly, we continue to use unimodal prediction loss in the first stage to improve the model training, and the multimodal trajectory loss is only applied to train the second-stage network.

4) *Handling multiple actor types*: Unlike earlier work [5] that mostly focused on a single traffic actor type, we model behavior of multiple actor types simultaneously, focusing on vehicles, pedestrians, and bicyclists. This is done by separating three sets of outputs, one for each type, after the backbone network computes the shared BEV learned features shown in Fig. 2. Handling all actors using a single model and in a single pass simplifies the SDV system significantly, and helps ensure safe and effective operations. It is important to emphasize that in the case of pedestrians and bicyclists we found that a unimodal output results in the best performance, and we do not use the multimodal loss nor the refinement stage for these traffic actors. Thus, in our experiments we set $M = 3$ for vehicles and $M = 1$ for the other actor types. Then, the final loss of the model is the sum of per-type losses, with each per-type loss comprising the detection loss as described in Sec. III-A.3, as well as the uncertainty-aware trajectory loss described in Sec. III-B.2 and Sec. III-B.3.

IV. EXPERIMENTS

A. Experimental settings

Following earlier work [6], [13] we evaluated the proposed approach using the ATG4D data set. The data was collected by a fleet of SDVs across several cities in North America using a 64-beam, roof-mounted lidar sensor. It contains over 1 million frames collected from 5,500 different scenarios, each scenario being a sequence of 250 frames captured at 10Hz. The labels are precise tracks of 3D bounding boxes at a maximum range of 100 meters from the data-collecting vehicle. Vehicles are the most common actor type in the data set, with 3.2x fewer pedestrians and 15x fewer bicyclists.

We set the parameters of the BEV image to $L = 150m$, $W = 100m$, $V = 3.2m$, $\Delta_L = 0.16m$, $\Delta_W = 0.16m$, $\Delta_V = 0.2m$, and use $T = 10$ sweeps to predict $H = 30$ future states at 10Hz (resulting in predictions that are 3s long). For the second stage, we cropped a $40m \times 40m$ region around each actor. The models were implemented in PyTorch

[39] and trained end-to-end with 16 GPUs, a per-GPU batch size of 2, Adam optimizer [40], and an initial learning rate of $2e-4$, training for 2 epochs completing in a day. Note that early in training the first-stage detection output is too noisy to provide stable inputs for the second-stage refinement. To mitigate this issue we used the ground-truth detections when training the second-stage network for the first 2.5k iterations.

We compared the discussed approaches to our implementation of IntentNet [5] which we extended to support multiple classes and tuned to obtain better results than reported in the original paper. In addition, using the published results we compared to the recently proposed end-to-end SpAGNN method that takes into account interactions between the traffic actors [6]. We evaluated the methods using both detection and prediction metrics. Following earlier literature for detection metrics, we set the IoU detection matching threshold to 0.7, 0.1, 0.3 for vehicles, pedestrians, and bicyclists, respectively. For prediction metrics we set the probability threshold to obtain a recall of 0.8 as the operational point, as in [6]. In particular, we report average precision (AP) detection metric, as well as displacement error (DE) [41] and cross-track (CT) prediction error at 3 seconds. For the multimodal approaches we report both the min-over- M metrics [11], [17] taking the minimal error over all modes (measuring recall) and the performance of the highest-probability mode (measuring precision).

B. Results

In this section we present the quantitative results of the competing methods. The evaluation results for vehicles, pedestrians, and bicyclists are summarized in Table I with best prediction results shown in bold, where we compare the proposed MultiXNet model to the state-of-the-art methods SpAGNN [6] and IntentNet [5]. Note that, in addition to the baseline IntentNet that uses displacement error (DE) in its loss, we also include a version of IntentNet with equally-weighted AT and CT losses instead. This is an extension of the baseline that uses the idea presented in Sec. III-B.1, which was shown to perform well in our experiments.

We can see that all methods achieved similar detection performance across the board. Comparing the state-of-the-art methods SpAGNN and IntentNet, the latter obtained better prediction accuracy on vehicle actors. The authors of SpAGNN did not provide results on other traffic actors so these results are not included in the table. Moreover, we see that IntentNet with AT/CT losses, corresponding to the model described in Sec. III-A that does not model the uncertainty, achieved comparable DE and CT errors as the original IntentNet with DE loss, with slightly improved results for vehicles and bicyclists. While the improvements are not large, this model allows for different weighting of AT and CT error components. This trade-off is an important feature for deployed models in autonomous driving, where prediction accuracies along these two directions may have different importance for the SDV (e.g., in merging scenarios AT may be more important, while when passing we may care more about CT). Lastly, the proposed MultiXNet outperformed

TABLE I: Comparison of approaches using the highest-probability mode, with detection performance evaluated using average precision in % (AP) and prediction using final displacement error (DE) and cross-track error (CT) at 3s in centimeters; results computed on the best-matching mode (i.e., min-over- M) for multimodal methods shown in parentheses where available

Method	Vehicles			Pedestrians			Bicyclists		
	AP	DE	CT	AP	DE	CT	AP	DE	CT
SpAGNN	83.9	96.0	-	-	-	-	-	-	-
IntentNet (DE)	84.0	90.5	26.3	88.2	61.9	32.6	83.8	53.0	23.7
IntentNet (AT/CT)	83.9	90.4	26.0	88.4	61.8	32.9	83.2	51.7	23.5
MultiXNet	84.2	83.1 (82.1)	20.2 (19.8)	88.4	57.2	30.5	84.6	48.5	20.7

TABLE II: Ablation study of the proposed MultiXNet; “Unc.” denotes uncertainty loss from Sec. III-B.1, “2nd” denotes the refinement stage from Sec. III-B.2, and “Mm.” denotes the multimodal loss from Sec. III-B.3

Unc.	2nd	Mm.	Vehicles			Pedestrians			Bicyclists		
			AP	DE	CT	AP	DE	CT	AP	DE	CT
			83.9	90.4	26.0	88.4	61.8	32.9	83.2	51.7	23.5
✓			84.1	91.9	22.8	88.2	57.1	30.4	84.6	49.9	21.1
	✓		84.6	82.2	22.2	88.7	63.2	33.2	84.3	51.6	23.8
✓	✓		84.4	83.3	20.4	88.4	57.6	30.6	83.9	52.0	21.7
	✓	✓	84.0	82.4 (81.4)	22.4 (21.8)	88.5	62.6	33.0	84.2	51.2	23.7
✓	✓	✓	84.2	83.1 (82.1)	20.2 (19.8)	88.4	57.2	30.5	84.6	48.5	20.7

the competing methods by a significant margin on all three actor types. Taking only vehicles into account, we see that modeling multimodal trajectories led to improvements when considering the min-over- M mode (result given in parentheses), as well as the highest-probability mode, indicating both better recall and better precision of MultiXNet, respectively.

In Table II we present results of an ablation study of the MultiXNet improvements, involving the components discussed in Sec. III-B. Note that the first row corresponds to the *IntentNet* (AT/CT) method from the Table I, while the last row corresponds to MultiXNet. We can see that all methods had nearly the same AP, which is not a surprising result since all approaches have identical detection architectures. Focusing on the vehicle actors for a moment, we see that modeling uncertainty led to improvements in the CT error, which decreased by 13%. Introducing the actor refinement using the second-stage network resulted in the largest improvement in the DE, leading to a drop of 11%. Note that such large improvements in DE and CT may translate to significant improvements in the SDV performance. The last three rows give performance of different variants of the second-stage model. Similarly to the result given previously, modeling for uncertainty led to substantial improvement of nearly 10% when it comes to the CT error. This can be explained by the fact that outliers are downweighted due to their larger variance as shown in equation (4), and thus have less impact during training as compared to the case when the variance is not taken into account.

Lastly, in the last two rows we evaluated the models that output multimodal trajectories. We see that using the highest-probability mode to measure performance gave comparable results to a unimodal alternative. This is due to a known limitation of such an evaluation scheme, which can not ad-

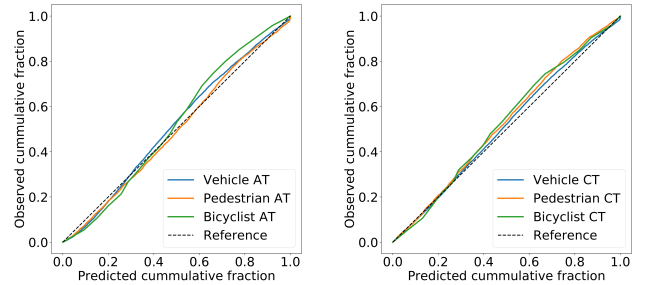


Fig. 3: Reliability diagrams for along-track (AT) (left) and cross-track (CT) (right) dimensions at 3s prediction horizon

equately capture the performance of multimodal approaches [11], [17]. For this reason we also report min-over- M shown in the parentheses, a commonly used multimodal evaluation technique in the literature, which indicated improvements in both DE and CT compared to the other baselines.

Let us discuss the results on pedestrians and bicyclists shown in the remainder of Table II. As explained in Sec. III-B.4, we did not use the second-stage refinement nor the multimodal loss for these actors, and the changes indicated in the *2nd* and *Mm.* columns only affected the vehicle branch of the network (results for the same setup changed slightly due to random weight initialization). Similar to the experiments with vehicles we see that modeling uncertainty led to improved results, with CT improvements between 9% and 13%, as seen in the second, fourth, and sixth rows.

In addition to improved performance, modeling uncertainty also allows reasoning about the inherent noise of future traffic movement. As mentioned in Sec. I, this is

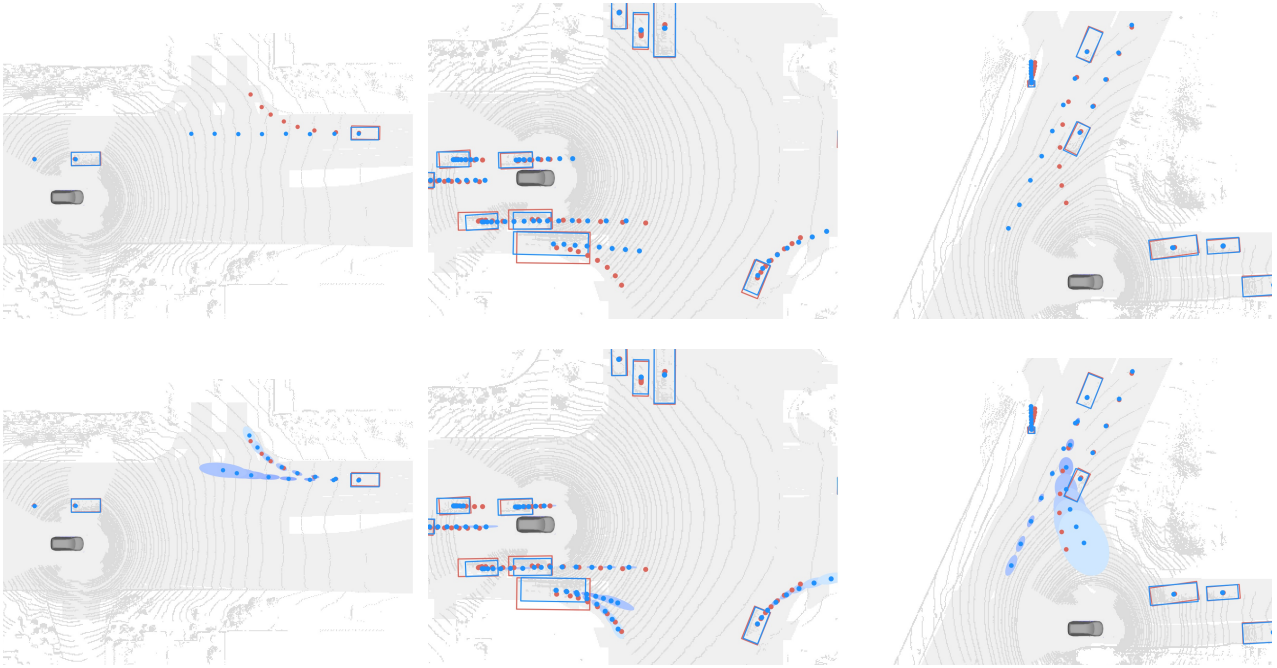


Fig. 4: Qualitative results of the competing models, top row: IntentNet, bottom row: MultiXNet; ground truth shown in red, predictions shown in blue, while colored ellipses indicate one standard deviation of inferred uncertainty for future predictions

an important feature to better allow downstream motion planning components to generate safe and efficient SDV motions. In Fig. 3 we provide reliability diagrams [10] along the AT and CT dimensions for all three actor types, measured at the prediction horizon of 3 seconds. We can see that the learned uncertainties were well calibrated, with slight under-confidence for all traffic actors. Bicyclist uncertainties were the least calibrated, followed by pedestrians. As expected, we observed that the actor types with the most training data showed the best calibrated uncertainties.

C. Qualitative results

In this section we present several representative case studies, exemplifying the benefits of the proposed MultiXNet over the state-of-the-art IntentNet. Three comparisons of the two methods are shown in Fig. 4, where we do not visualize low-probability MultiXNet trajectories below 0.3 threshold.

In the first case we see an actor approaching an intersection and making a right-hand turn, where unimodal IntentNet incorrectly predicted that they will continue moving straight through the intersection. On the other hand, MultiXNet predicted a very accurate turning trajectory with high certainty, while also allowing for the possibility of going-straight behavior. Apart from the predictions, we can see that both models detected the two actors in the SDV’s surroundings with high accuracy. In the second case, the SDV is moving through an intersection with a green traffic light, surrounded by vehicles. We can see that both models correctly detected and predicted the movements of the majority of the traffic actors. Let us consider motion prediction for a large truck in a right-turn lane on the SDV’s right-hand side. Again, IntentNet predicted a straight trajectory while in actuality the actor made a turn. As before, MultiXNet generated multiple

modes and provided reasonable uncertainty estimates for both the turning and the going-straight trajectories.

Lastly, the third case shows the SDV in an uncommon three-way intersection. As previously, both models provided accurate detections of the surrounding actors, including one pedestrian in the top of the scene. Let us direct our attention to the actor approaching the intersection from the upper part of the figure. This actor made an unprotected left turn towards the SDV, which IntentNet mispredicted. Conversely, we see that MultiXNet produced both possible modes, including a turning trajectory with large uncertainty due to the unusual shape of the intersection.

V. CONCLUSION

In this work we focused on the critical tasks of object detection and motion prediction for a self-driving system, and described an end-to-end model that addresses both tasks within a single framework. Existing state-of-the-art models are suboptimal as they do not reason about the uncertainty of future behavior, nor the multimodality of the future movement of traffic actors. To address these disadvantages we introduced MultiXNet, a multistage model that first infers object detections and predictions, and then refines these predictions using a second stage to output multiple potential future trajectories. In addition, the model estimates cross- and along-track movement uncertainties, which are critical for ensuring safety in downstream modules of the SDV system. The proposed method was evaluated on a large-scale data collected on the streets of several US cities, where it outperformed the existing state-of-the-art. The results strongly suggest the practical benefits of the proposed architecture.

REFERENCES

- [1] P. Stahl, B. Donmez, and G. A. Jamieson, "Anticipation in driving: The role of experience in the efficacy of pre-event conflict cues," *IEEE Transactions on Human-Machine Systems*, vol. 44, no. 5, pp. 603–613, 2014.
- [2] —, "Supporting anticipation in driving through attentional and interpretational in-vehicle displays," *Accident Analysis & Prevention*, vol. 91, pp. 103–113, 2016.
- [3] A. Cosgun, L. Ma, et al., "Towards full automated drive in urban environments: A demonstration in gomentum station, california," in *IEEE Intelligent Vehicles Symposium*, 2017, pp. 1811–1818. [Online]. Available: <https://doi.org/10.1109/IVS.2017.7995969>
- [4] W. Luo, B. Yang, and R. Urtasun, "Fast and furious: Real time end-to-end 3d detection, tracking and motion forecasting with a single convolutional net," in *Proceedings of the IEEE CVPR*, 2018, pp. 3569–3577.
- [5] S. Casas, W. Luo, and R. Urtasun, "Intentnet: Learning to predict intention from raw sensor data," in *Conference on Robot Learning*, 2018, pp. 947–956.
- [6] S. Casas, C. Gulino, R. Liao, and R. Urtasun, "Spatially-aware graph neural networks for relational behavior forecasting from sensor data," *arXiv preprint arXiv:1910.08233*, 2019.
- [7] G. P. Meyer, J. Charland, S. Pandey, A. Laddha, C. Vallespi-Gonzalez, and C. K. Wellington, "Laserflow: Efficient and probabilistic object detection and motion forecasting," *arXiv preprint arXiv:2003.05982*, 2020.
- [8] F.-C. Chou, T.-H. Lin, H. Cui, V. Radosavljevic, T. Nguyen, T.-K. Huang, M. Niedoba, J. Schneider, and N. Djuric, "Predicting motion of vulnerable road users using high-definition maps and efficient convnets," in *IEEE Intelligent Vehicles Symposium (IV)*, 2020.
- [9] Y. Chai, B. Sapp, M. Bansal, and D. Anguelov, "Multipath: Multiple probabilistic anchor trajectory hypotheses for behavior prediction," *arXiv preprint arXiv:1910.05449*, 2019.
- [10] N. Djuric, V. Radosavljevic, H. Cui, T. Nguyen, F.-C. Chou, T.-H. Lin, and J. Schneider, "Uncertainty-aware short-term motion prediction of traffic actors for autonomous driving," in *IEEE Winter Conference on Applications of Computer Vision (WACV)*, 2020.
- [11] H. Cui, V. Radosavljevic, F.-C. Chou, T.-H. Lin, T. Nguyen, T.-K. Huang, J. Schneider, and N. Djuric, "Multimodal trajectory predictions for autonomous driving using deep convolutional networks," in *2019 International Conference on Robotics and Automation (ICRA)*. IEEE, 2019, pp. 2090–2096.
- [12] A. H. Lang, S. Vora, H. Caesar, L. Zhou, J. Yang, and O. Beijbom, "Pointpillars: Fast encoders for object detection from point clouds," in *Proceedings of the IEEE Conference on Computer Vision and Pattern Recognition*, 2019, pp. 12 697–12 705.
- [13] G. P. Meyer, A. Laddha, E. Kee, C. Vallespi-Gonzalez, and C. K. Wellington, "Lasernet: An efficient probabilistic 3d object detector for autonomous driving," in *Proceedings of the IEEE Conference on Computer Vision and Pattern Recognition*, 2019, pp. 12 677–12 686.
- [14] G. P. Meyer, J. Charland, D. Hegde, A. Laddha, and C. Vallespi-Gonzalez, "Sensor fusion for joint 3d object detection and semantic segmentation," in *The IEEE Conference on Computer Vision and Pattern Recognition (CVPR) Workshops*, June 2019.
- [15] X. Chen, H. Ma, J. Wan, B. Li, and T. Xia, "Multi-view 3d object detection network for autonomous driving," in *Proceedings of the IEEE Conference on Computer Vision and Pattern Recognition*, 2017, pp. 1907–1915.
- [16] Y. Zhou, P. Sun, Y. Zhang, D. Anguelov, J. Gao, T. Ouyang, J. Guo, J. Ngiam, and V. Vasudevan, "End-to-end multi-view fusion for 3d object detection in lidar point clouds," *arXiv preprint arXiv:1910.06528*, 2019.
- [17] N. Lee, W. Choi, P. Vernaza, C. B. Choy, P. H. Torr, and M. Chandraker, "Desire: Distant future prediction in dynamic scenes with interacting agents," in *Proceedings of the IEEE Conference on Computer Vision and Pattern Recognition*, 2017, pp. 336–345.
- [18] B. Ivanovic and M. Pavone, "The trajectron: Probabilistic multi-agent trajectory modeling with dynamic spatiotemporal graphs," in *Proceedings of the IEEE International Conference on Computer Vision*, 2019, pp. 2375–2384.
- [19] T. Salzmann, B. Ivanovic, P. Chakraborty, and M. Pavone, "Trajectron++: Multi-agent generative trajectory forecasting with heterogeneous data for control," *arXiv preprint arXiv:2001.03093*, 2020.
- [20] A. Gupta, J. Johnson, L. Fei-Fei, S. Savarese, and A. Alahi, "Social gan: Socially acceptable trajectories with generative adversarial networks," in *Proceedings of the IEEE Conference on Computer Vision and Pattern Recognition*, 2018, pp. 2255–2264.
- [21] T. Zhao, Y. Xu, M. Monfort, W. Choi, C. Baker, Y. Zhao, Y. Wang, and Y. N. Wu, "Multi-agent tensor fusion for contextual trajectory prediction," in *Proceedings of the IEEE Conference on Computer Vision and Pattern Recognition*, 2019, pp. 12 126–12 134.
- [22] A. Sadeghian, V. Kosaraju, A. Sadeghian, N. Hirose, H. Rezatofighi, and S. Savarese, "Sophie: An attentive gan for predicting paths compliant to social and physical constraints," in *Proceedings of the IEEE Conference on Computer Vision and Pattern Recognition*, 2019, pp. 1349–1358.
- [23] V. Kosaraju, A. Sadeghian, R. Martín-Martín, I. Reid, H. Rezatofighi, and S. Savarese, "Social-bigat: Multimodal trajectory forecasting using bicycle-gan and graph attention networks," in *Advances in Neural Information Processing Systems*, 2019, pp. 137–146.
- [24] Y. Ma, X. Zhu, S. Zhang, R. Yang, W. Wang, and D. Manocha, "Trafficpredict: Trajectory prediction for heterogeneous traffic-agents," in *AAAI Conference on Artificial Intelligence*, 2019.
- [25] R. Chandra, U. Bhattacharya, A. Bera, and D. Manocha, "Trophic: Trajectory prediction in dense and heterogeneous traffic using weighted interactions," in *Proceedings of the IEEE Conference on Computer Vision and Pattern Recognition*, 2019, pp. 8483–8492.
- [26] Y. Yuan and K. Kitani, "Diverse trajectory forecasting with determinantal point processes," *arXiv preprint arXiv:1907.04967*, 2019.
- [27] T. Phan-Minh, E. C. Grigore, F. A. Boulton, O. Beijbom, and E. M. Wolff, "Covernet: Multimodal behavior prediction using trajectory sets," *arXiv preprint arXiv:1911.10298*, 2019.
- [28] H. Cui, T. Nguyen, F.-C. Chou, T.-H. Lin, J. Schneider, D. Bradley, and N. Djuric, "Deep kinematic models for physically realistic prediction of vehicle trajectories," *2020 International Conference on Robotics and Automation (ICRA)*, 2020.
- [29] J. Hong, B. Sapp, and J. Philbin, "Rules of the road: Predicting driving behavior with a convolutional model of semantic interactions," in *Proceedings of the IEEE Conference on Computer Vision and Pattern Recognition*, 2019, pp. 8454–8462.
- [30] A. Jain, S. Casas, R. Liao, Y. Xiong, S. Feng, S. Segal, and R. Urtasun, "Discrete residual flow for probabilistic pedestrian behavior prediction," *arXiv preprint arXiv:1910.08041*, 2019.
- [31] W. Zeng, W. Luo, S. Suo, A. Sadat, B. Yang, S. Casas, and R. Urtasun, "End-to-end interpretable neural motion planner," in *Proceedings of the IEEE Conference on Computer Vision and Pattern Recognition*, 2019, pp. 8660–8669.
- [32] P. Wu, S. Chen, and D. Metaxas, "Motionnet: Joint perception and motion prediction for autonomous driving based on bird's eye view maps," *arXiv preprint arXiv:2003.06754*, 2020.
- [33] T.-Y. Lin, P. Goyal, R. Girshick, K. He, and P. Dollar, "Focal loss for dense object detection," in *ICCV*, 2017.
- [34] C. Gong and D. McNally, "A methodology for automated trajectory prediction analysis," in *AIAA Guidance, Navigation, and Control Conference and Exhibit*, p. 4788.
- [35] G. P. Meyer, "An alternative probabilistic interpretation of the huber loss," *arXiv preprint arXiv:1911.02088*, 2019.
- [36] G. P. Meyer and N. Thakurdesai, "Learning an uncertainty-aware object detector for autonomous driving," *arXiv preprint arXiv:1910.11375*, 2019.
- [37] M. Liang, B. Yang, Y. Chen, R. Hu, and R. Urtasun, "Multi-task multi-sensor fusion for 3d object detection," in *Proceedings of the IEEE Conference on Computer Vision and Pattern Recognition*, 2019, pp. 7345–7353.
- [38] S. Ren, K. He, R. Girshick, and J. Sun, "Faster r-cnn: Towards real-time object detection with region proposal networks," in *Advances in neural information processing systems*, 2015, pp. 91–99.
- [39] A. Paszke, S. Gross, et al., "Pytorch: An imperative style, high-performance deep learning library," in *Advances in Neural Information Processing Systems* 32, H. Wallach, H. Larochelle, A. Beygelzimer, F. dAlché Buc, E. Fox, and R. Garnett, Eds. Curran Associates, Inc., 2019, pp. 8024–8035.
- [40] D. P. Kingma and J. Ba, "Adam: A method for stochastic optimization," *arXiv preprint arXiv:1412.6980*, 2014.
- [41] A. Alahi, K. Goel, V. Ramanathan, A. Robicquet, L. Fei-Fei, and S. Savarese, "Social lstm: Human trajectory prediction in crowded spaces," in *Proceedings of the IEEE conference on computer vision and pattern recognition*, 2016, pp. 961–971.